Bull. Pharm. Sci., Assiut University, Vol. 48, Issue 1, 2025, pp. 277-294.

Bulletin of Pharmaceutical Sciences
Assiut University
Website: http://bpsa.journals.ekb.eg/

BULL. PHARM. SCI. Assiut Univ.

UNVEILING THE PHARMACOLOGICAL POTENTIAL OF *HYPERICUM PERFORATUM* DERIVED COMPOUNDS AGAINST ALZHEIMER'S DISEASE: INSIGHTS FROM COMPUTATIONAL AND DYNAMICS STUDIES

Adel Alghamdi*

Department of Pharmaceutical Chemistry, Faculty of Pharmacy, Al-Baha University, P.O. Box 1988 Al-Baha, Saudi Arabia

The worldwide health care system is significantly threatened by Alzheimer's disease (AD), which arises from a combination of conditions leading to neuronal malfunction, memory impairment, and cognitive decline. Hypericum perforatum, often known as St. John's wort, has garnered significant attention due to its possible therapeutic advantages in the treatment of neurodegenerative diseases. The lack of efficacious treatments for diseases such as Alzheimer's and Parkinson's disease is becoming a growing global health issue. This study investigated the therapeutic potential of five reported phytochemicals of this plant including hypericin (HP-1), biapigenin (HP-2), kaempferol (HP-3), hyperforin (HP-4), hyperocide (HP-5), based on their binding affinity with AD-associated proteins namely acetylcholinesterase (AChE) and butyrylcholinesterase (BChE). The Glide-XP module from Schrödinger was utilized to conduct thorough docking investigations, which were then followed by molecular dynamic (MD) simulations using IMods. The selected compounds were subjected to docking analysis to determine the binding energies of their interactions with the target proteins. Additionally, molecular dynamics (MD) simulations were conducted to confirm the stability of the bound complexes. The top hits among the five selected phytochemical compounds, HP-2 (-7.461 kcal/mol) and HP-1 (-7.304 kcal/mol), have the greatest docking scores for the AChE enzyme. Similarly, in case of BChE enzyme, the phytochemicals HP-5 (-7.991 kcal/mol) and HP-3 (-7.849 kcal/mol) have substantial binding affinities. Through the different online tools including swissADME, pkSCM, stoptox, molinspiration, and swiss target prediction analysis, the selected compounds' pharmacokinetic characteristics, drug likeness, toxicity, bioactivity score prediction, and enzyme target prediction were also examined.

Keywords: *Hypericum perforatum; phytochemicals; neurological disorders; fingerprinting analysis; docking; MD simulations*

INTRODUCTION

The utilization of natural products as therapeutic agents for health management and treatment of common disorders has been a longstanding practice due to their inherent health-promoting capabilities and the presence of bioactive components[1]. I As per the World Health Organization, a significant proportion of the global population, approximately 80%, primarily relies on conventional and herbal drugs. In numerous countries, the overall consumption of medicinal substances is estimated to range from 30% to 50%, primarily derived from the preparation of conventional medicine[1.2]. In Germany, it has been shown that almost 90% of the population has employed traditional natural therapies for various health conditions. Therefore, the utilization of traditional medicine is widespread in both industrialized and developing nations[3]. The global market for the utilization of traditional medicine is experiencing significant growth.

Received : 21/9/2024 & Accepted : 17/12/2024

*Corresponding author: Adel Alghamdi, E-mail: ai.alghamdi@bu.edu.sa

The annual expenditure on herbal medicine exceeds $60 billion and is steadily rising[3].

Alzheimer's disease (AD) is a degenerative neurological condition that is the predominant etiology of dementia[4], It impacts a minimum of 27 million individuals and constitutes 60 to 70% of all instances of dementia[5]. he condition is classified as progressive due to the gradual deterioration of symptoms over time[6]. According to Abraham, Maharifa, et al. (2022), throughout its most extreme stages, this disease results in the progressive decline of cognitive function, brain cells, and memory, rendering individuals entirely reliant on external support for their survival[7]. Despite almost a century of research and disease identification, a comprehensive cure for this disorder has yet to be developed[8]. Throughout history, *H. perforatum*, commonly referred to as St. John's wort, has been employed as a conventional herbal remedy, specifically for the management of various afflictions such as inflammation and mood disorders. Nevertheless, the scientific community has just started to recognize the potential neuroprotective properties of this substance, specifically in relation to neurodegenerative diseases[9,10]. A comprehensive review by Suryawanshi et al. (2024) delves into the pharmacognosy and preclinical studies of *H. perforatum*, highlighting its putative molecular mechanisms and clinical relevance in neurodegenerative disorders such as AD[9]. The computer-aided in silico technique has been widely employed in the initial stages of drug research with the aim of searching for possible treatments. The investigation of the structures and functions of biological targets is a fundamental aspect of computer-aided rational drug design, which aims to identify novel treatments[11]. The technique described by Alom, Bonna et al. (2023) is a valuable approach for forecasting possible drug candidates for various diseases in a manner that is both cost-effective and time-efficient, while also reducing errors during the final stages[12]. The present investigation centres on examining the specific efficacy of phytochemicals derived from *H. perforatum* against the AChE and BChE proteins through the utilization of ADMET, molecular docking, and molecular simulation analysis techniques. This research endeavor aims to elucidate the primary phytochemical responsible for the therapeutic properties of H. *perforatum*, as well as determine if the neuroprotective activity of *H. perforatum* is attributed to a singular phytochemical or a synergistic effect resulting from the combined action of multiple phytochemicals.

MATERIAL AND METHODS

Protein Retrieval and Preparation (protein model preparation)

The co-crystal structures of acetylcholinesterase (AChE) and butyrylcholinesterase (BChE) were obtained from the RCSB Protein Data Bank protein structures with PDB ID's 4EY6 and 7AIY, respectively. Before the docking process, protein structures were meticulously prepared, involving the exclusion of solvent molecules, correction of absent atoms, and geometric optimization, to preserve the structural integrity and enhance the reliability of the protein models[13].

Ligand Retrieval and Preparation (library preparation)

A total of five bioactive compounds including hypericin (HP-1), biapigenin (HP-2), kaempferol (HP-3), hyperforin (HP-4), hyperocide (HP-5) as reported from the plant[9] were selected as ligands. 3D structures of these compounds were obtained from PubChem database (https://pubchem.ncbi.nlm.nih.gov/) in sdf format. The structures of ligands were prepared using the Open Babel[33] soft- ware that is included as a default option in the PyRx.

Molecular Docking

To anticipate the binding affinity between a ligand and its target protein, molecular docking uses the docking score to evaluate the ligand's active conformation with the protein. Molecular docking is frequently employed to anticipate how chemicals will bind to proteins. In particular, flexible docking helps enhance the specificity of ligand binding inside an active site of a protein. Before the docking process began, the proteins were cleaned of any co-crystallized water and hetero atoms. Molecular docking was carried out by Glide-XP module from Schrödinger to explore all possible orientations, conformations, and

binding affinities for the ligands with AChE and BChE active site.

The selected compounds, including hypericin (HP-1), biapigenin (HP-2), kaempferol (HP-3), hyperforin (HP-4), hyperocide (HP-5), were subjected to flexible docking into the active site of AChE and BChE employing the Glide-XP module from Schrödinger[14] , in accordance with established protocols[15-17]. The receptor grid was constructed using the preprocessed protein, applying the OPLS 2005 force field. Adjustments to the *van der Waals* (*vdW*) radii of protein atoms were made using a scaling factor of 1.0, and a charge cutoff of 0.25 was implemented to assess polarity. The dimensions of the receptor grid box were defined as ≤ 20Å in each spatial direction (x, y, and z), centering the box around the target ligands to ensure ample space in the binding pocket for accommodating any ligand[26]. A cubic docking grid, positioned near the hinge residue M769 and tailored to enclose ligands up to ≤ 20Å, was generated. Glide's extra precision (XP) scoring mechanism was employed, allowing for complete ligand flexibility during docking. The final energy assessment was conducted using GlideScore, yielding the most favorable pose for each of the five compounds[18]. Remarkably, the docking simulations frequently converged, indicating the lowest energy docked complex for the most similar conformations.

***Structural Interaction Fingerprinting* (SIFt) analysis**

SIFt represents an innovative approach for modeling and assessing three-dimensional interactions between proteins and ligands. Through SIFt approach, a binary digit interaction fingerprint is generated, translating the three-dimensional structural binding characteristics of a ligand-protein complex. Each fingerprint encapsulates the "structural interaction pattern" of the complex, facilitating the organization, analysis, and presentation of extensive data within ligand-receptor complexes, thereby enabling efficient database mining.[19]. SIFt panel in Schrodinger suite 2020-3 was used to generate the interaction fingerprint of five docking complexes of the selected phytochemicals. The input files chosen were the receptor grid and ligands. After generating the fingerprint, the outcome can be represented in an Excel spreadsheet, which emphasizes the residues and interaction types, such as hydrophobic, H-bond donor, and H-bond acceptor features, that have the most impact on the binding process. The types of interaction exhibited by the residues were denoted using corresponding colors, while the presence and lack of interaction were represented by the numerals 1 and 0, respectively[20]. More details for generating SIFt model can be found in previously published research[18.21].

Pharmacokinetics evaluation

ADME, pkCSM and Toxicity Analysis

Adsorption, Distribution, Metabolism, Excretion, and Toxicity are the acronyms used to denote scientific concepts. The document encompasses the pharmacokinetic characteristics of a substance, namely a therapeutic molecule, and holds considerable importance in the assessment of its pharmacodynamic properties. The SWISS ADMET website was used to identify the attributes of the active compounds, including their intestinal absorption, distribution, metabolism, and excretion properties, considering all the compounds that were provisionally identified[22]. The pkCSM-pharmacokinetics web tool, which is readily available, represents an innovative approach to forecasting and enhancing the ADME/Tox characteristics of small molecules. This tool utilizes graph-based signatures and experimental data as its foundation. The molecular structures of the compounds that were tentatively identified, as reported in **Table 1**, were incorporated into the ADME/Tox web tools SwissADME and pkCSM-pharmacokinetics using the simplified molecular-input line-entry specification (SMILES) nomenclature. The ADME/Tox attributes that were deemed significant by the web tools were chosen to represent the ADME/Tox profile, as outlined by Pires, Blundell et al. (2015)[23].

The StopTox server was utilized for doing toxicity assessments[24]. The StopTox server employs a collection of quantitative structure-activity relationship (QSAR) models to assess the toxicity of compounds across different toxicity endpoints, such as acute inhalation

toxicity, acute oral toxicity, eye irritation and corrosion, and skin sensitization. This evaluation is conducted by compiling, curating, and integrating the most extensive publicly accessible datasets.

Bioactivity Score and drug target class prediction

A drug is intended to form a chemical bond with a specific biological target. Enzymes, ion channels, and receptors are examples of biological targets. The assessment of the bioactivity of phytocompounds can be conducted by determining the activity score of various biomarkers, including GPCR ligand, ion channel modulator, nuclear receptor ligand, kinase inhibitor, protease inhibitor, and enzyme inhibitor. The molinspiration chemoinformatics software was utilized to verify all the parameters[31]. The miscreen engine of the Molinspiration tool initially examines a training dataset consisting of active structures. of many instances, even a solitary active molecule is deemed adequate for constructing a functional model. Subsequently, the engine use advanced Bayesian statistics to compare this dataset with inactive molecules. The training process only requires the SMILES or SDF structures of active phytocompounds, without the need for information regarding the active site or binding mechanism[26]. Organic molecules have a probability of being active if their bioactivity score is greater than 0, moderately active if it falls between 5.0 and 0.0, and inert if it falls below 5.0[32]. The prediction of drug target class and structurally related analogs. The researchers employed the Swiss Target Prediction service to forecast probable macromolecular targets for the most promising candidates, as described by Daina, Michielin et al. (2019)[25]. The server employs a collection of 376,342 bioactive compounds that have been found on around 3068 proteins, utilizing both 2D and 3D similarity as the basis for comparison.

Table 1: Chemical structures (2d and 3D), SMILES, and docking scores of the selected phytochemicals of *Hypericum perforatum* against the tested enzymes.

Ligands/Standard	Smiles	Structures		Docking Scores	
		2d	3d	AChE	BChE
HP-1	CC1=CC(=O)C2=C(C3=C(C=C(C4=C3C5=C2C1=C6C(=CC(=O)C7=C(C8=C(C=C(C4=C8C5=C67)O)O)O)O)C)O)O)O	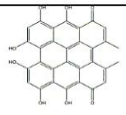	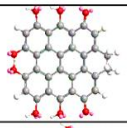	-7.304	-6.34
HP-2	C1=CC(=CC=C1C2=CC(=O)C3=C(O2)C(=C(C=C3O)O)C4=C(OC5=CC(=CC(=C5C4=O)O)O)C6=CC=C(C=C6)O)O	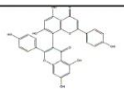	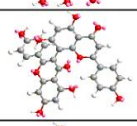	-7.461	-7.418
HP-3	C1=CC(=CC=C1C2=C(C(=O)C3=C(C=C(C=C3O2)O)O)O)O	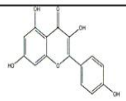	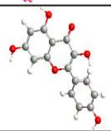	-5.14	-7.849
HP-4	CC(C)C(=O)C12C(=O)C(=C(C(C1=O)(CC(C2(C)C)CCC=C(C)C)CC=C(C)C)CC=C(C)C)O)CC=C(C)C	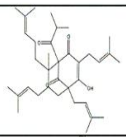	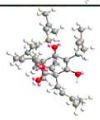	-4.018	-7.369
HP-5	C1=CC(=C(C=C1C2=C(C(=O)C3=C(C=C(C=C3O2)O)O)O)OC4C(C(C(C(O4)CO)O)O)O)O)O	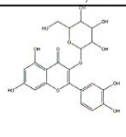	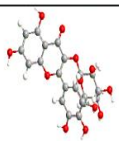	-4.054	-7.991
Eserine	CC12CCN(C1N(C3=C2C=C(C=C3)OC(=O)NC)C)C	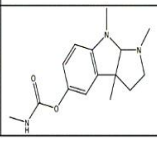	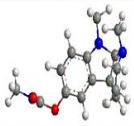	-6.733	-5.006

DFT studies (MESP/HOMO/LUMO analysis)

The DFT calculations were performed with slight modification using the previously described protocol[26]. Utilizing the Gaussian 06 package (Rev.E.01) with the default configuration, all calculations in the SVP basis set utilized the B3LYP function. Using this theory, the electronic structure of atoms and molecules can be effectively calculated. The present investigation will ascertain the optimized geometric parameters, molecular electrostatic potential (MEP), frontier molecular orbital (FMO), and global and local reactivity descriptors. The checks were examined utilizing Guass View 6.

Molecular Dynamics (MD) simulations

The molecular dynamic analysis was performed on the selected docking complex with the lowest energy value and best-posed conformation, utilizing the docking data. Molecular dynamics (MD) aims to numerically simulate the condensed phases of a molecular system to understand, predict, and compute its parameters[27]. The stability of the target was determined using molecular dynamics (MD) simulations, employing the most optimal natural product molecule. The MD simulations were conducted using the iMod server (iMODS) available at https://imods.iqfr.csic.es. The iMod server offers a user-friendly interface for the enhanced normal mode analysis (NMA) technique in inner coordinates. All prominent web browsers, along with modern mobile devices, exhibit a high level of responsiveness and spontaneity in their online interface. Users can employ molecular dynamics (MD) or non-molecular dynamics (NMA) to simulate potential paths between two conformations. They can then actively investigate the resulting structures, trajectories, animations, and even huge macromolecules, all inside a three-dimensional (3D) environment.[27].

RESULTS AND DISCUSSION

Results

Molecular docking analysis

The generation of a diverse range of phytochemicals by plants is widely recognized for their pharmacological significance and potential as therapeutic agents for the treatment and prevention of many ailments[28]. Research interests have stimulated the exploration of some commonly utilized therapeutic plants. The medicinal plants provide a plethora of bioactive chemicals, rendering them suitable for the production of functional meals and pharmaceuticals. Extensive in-silico approaches have been used to predict the interaction between key phytochemicals and target proteins. To determine the affinities between lead-like compounds and the target protein, molecular docking is considered the most appropriate approach. This study employs docking of five selected phytochemical compounds, retrieved from one of the important medicinal plant traditionally used against different neurological problems, against the enzymes AChE (PDB ID: 4EY6), and BChE (PDB ID: 7AIY)) using lide-XP module from Schrödinger[14] , in accordance with established protocols[15-17]. Multiple investigations have documented the inhibitory interaction of natural phytochemical compounds derived from different sources with these proteins. Nevertheless, there is a dearth of research investigating the possible utilization of prevalent phytochemicals derived from this particular plant for the purpose of managing neurological illnesses. The chemical structures of bioactive hits selected for molecular docking analysis are shown in **Fig. 1 B**, while the chemical structures of standard compounds Eserine (**Fig. 1 A**), as well as the Binding conformation of selected hits and standard compounds in their corresponding molecular targets is presented in **Fig. 1 C**. From the results of docking in this study, binding free energies were observed from lowest to highest values. Out of the five selected phytochemical compounds, the top hits, namely HP-2 (-7.461 kcal/mol), HP-1 (-7.304 kcal/mol) have the highest docking scores for the AChE enzyme. Likewise, in case of BChE enzyme, the phytochemicals HP-5 (-7.991 kcal/mol) and HP-3 (-7.849 kcal/mol) we having strong binding affinities (**Table 1**). To investigate variations in docking scores resulting from diverse interaction patterns, we captured and visually portrayed the optimal docking conformations for each compound (HP-1 to HP-5). Notably, top-ranked ligands, along with their interactions with proteins and corresponding standard inhibitors, share a common binding cavity. The selection of the

best compound for each enzyme is based on both the highest docking scores and their interactions, specifically the number of hydrogen bonds, with residues within the binding cavity (**Fig. 2** and **Fig. 3**). In the AChE-HP1 bonded system, the residues within the binding cavity include E73, D72, V71, Q74, Y70, Y334, F331, Y121, I287, F290, F288, R289, S286, W279, and L282 (**Fig. 2**). Likewise, for the binding cavity of AChE-HP2, complex is constituted by residues including L358, R289, F290, I287, F284, D285, L282, N280, W279, E73, Q74, D72, Y334, F330, A336, F331, and G335. Similarly, as indicated in the **Fig. 6**, the amino acid residues of the BChE-HP3 complex were noted to have S287, L286, W231, V288, Q119, T120, G116, W82, G115, E197, 1442, G439, H438, A199, S198, F329, and F398. For the BChE-HP5 complex, there were S198, E197, H438, G439, M437, Y440, W430, W82, Y332, P285, Q119, S287, V288, W231, A199, L286, S198, and E197 amino acid residues (**Fig. 3**). In summary, our research findings, derived from docking experiments, reveal that natural phytochemical compounds derived from the chosen plant exhibit robust binding affinity towards the targeted proteins at the inhibitory active binding region.

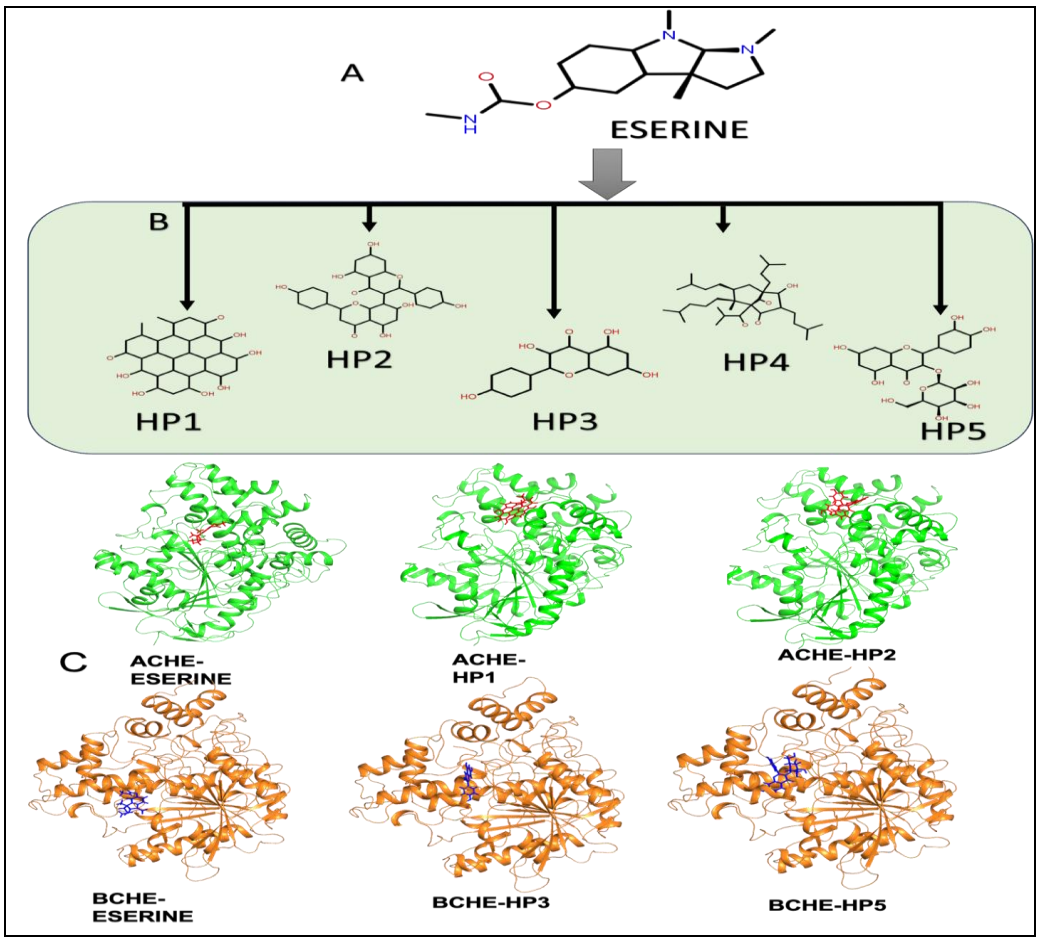

Fig. 1: Chemical structures of bioactive hits selected for molecular docking analysis. (A) Chemical structures of standard compounds Eserine (ACB). (B) 2D-structural representation of selected bioactive molecules. (C) Binding conformation of selected hits and standard compounds in their corresponding molecular targets.

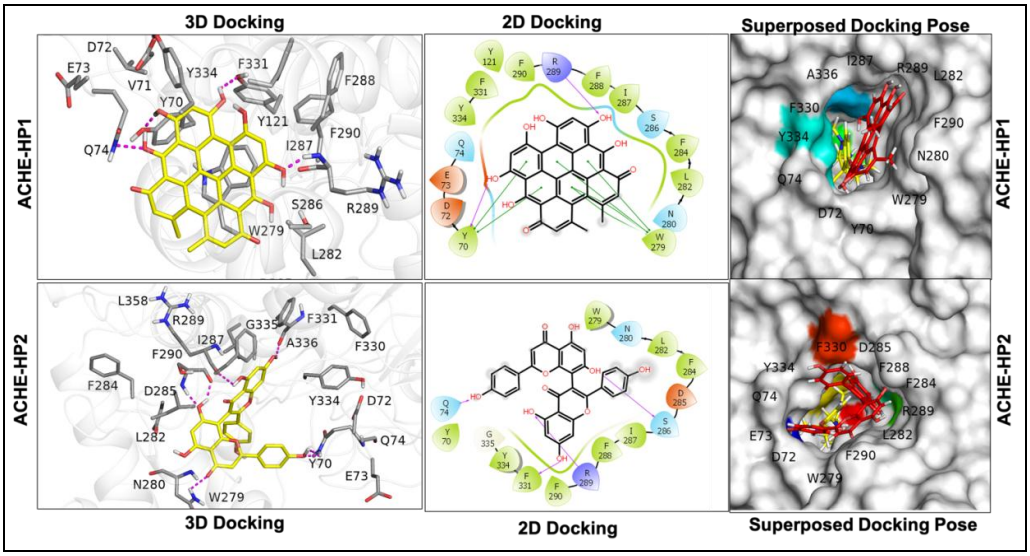

Fig. 2: Docking generated complexes (2D, 3D, and superposed docking pose images) of AChE enzymes bonded to their respective phytocompound with lowest docking scores.

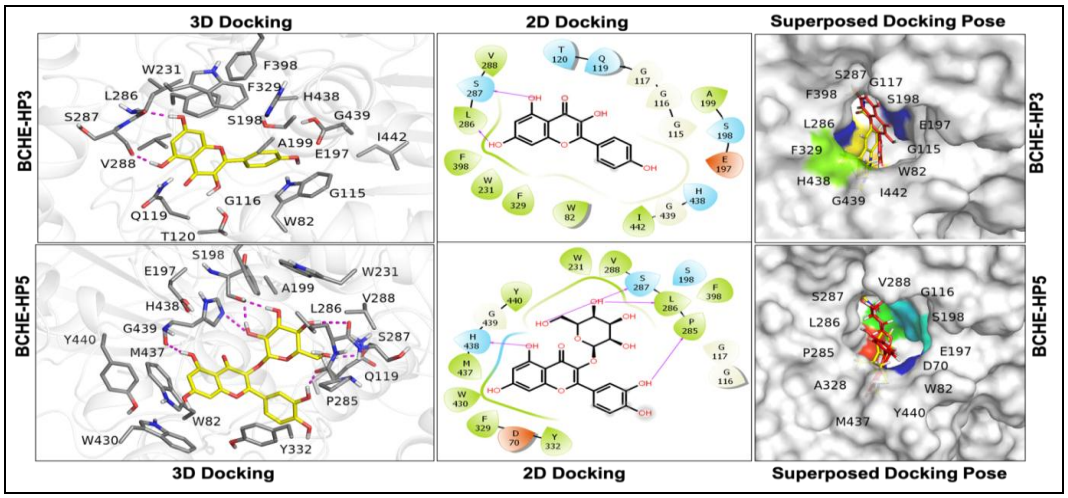

Fig. 3: Docking generated complexes (2D, 3D, and superposed docking pose images) of BChE enzymes bonded to their respective phytocompound with lowest docking scores.

Structural Interaction Fingerprinting (SIFt) parameters

Assessing the docking orientations of potential new ligands and comparing them to interactions in known protein-ligand complexes, interaction fingerprints offer an efficient method for creating customized scoring systems designed specifically for a particular protein of interest.[29]. By considering only the interactions and ignoring the molecular structure, this approach is capable of identifying new ligands that possess similar interactions but unique core structures. This procedure, which is called "scaffold hopping," is vital to medicinal chemistry[30]. Several interaction fingerprints have been developed and successfully employed in the preceding literature to elucidate docking postures[31]. SIFt, or structural interaction fingerprint, is among the earliest and most widely recognized fingerprints. A binary fingerprint is generated for each amino acid, consisting of a seven-bit vector. This fingerprint delineates the interaction pattern between the residue and the ligand. It specifies whether the residue acts as a hydrogen bond donor or acceptor, the interaction type (any contact, hydrophobic, or aromatic), and whether either the main chain or side chain atoms (or both) are involved[32].

The number of hydrogen bond donor, acceptor, and hydrophobic interactions between ligands and the AChE and BChE

receptor is shown in the **Fig. 4** and **5**, respectively. For the AChE enzyme and ligand complexes, it was noted that the amino acid residues including Q74 and L282 were invloved in hydrogen bon acceptor interaction, while the residues Y121, and N280 were noted to have the hydrogen bon donor interacction (**Fig. 4**). Similary, in the case of fingerprinting for the BChE enzyme as presented in the **Fig. 5**, the hydrogen bond donor residues observed to interact the most with the ligands were S198, Q197, D70, N83, and F398. Our findings implied that S198 is a crucial residue that might be the subject of additional research examining the relationship between structure and function. Hydrophobic interactions were observed with the following residues: N68, G78, G115, G116, Y128, S287, V288, R332, M437, and Y440. It is interesting to note that the compounds suggested as potential candidates from this study were seen to interact with experimentally determined active site residues of AChE and BChE proteins. This interaction suggests the compounds may have a high binding affinity.

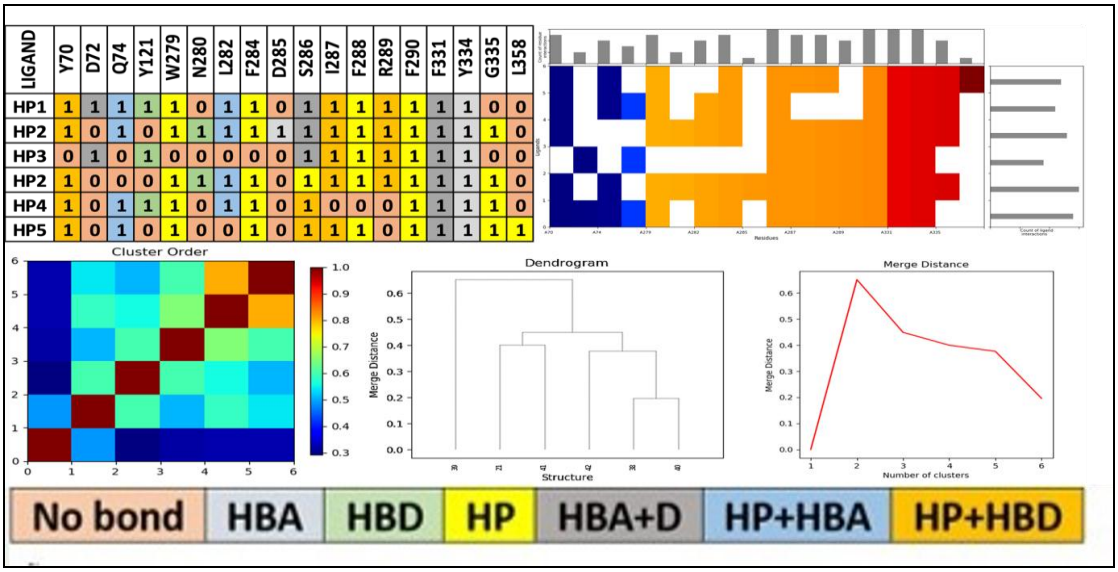

Fig. 4: Structural interaction fingerprinting (Sift) of the selected phytochemicals of *Hypericum perforatum* with AChE enzyme.

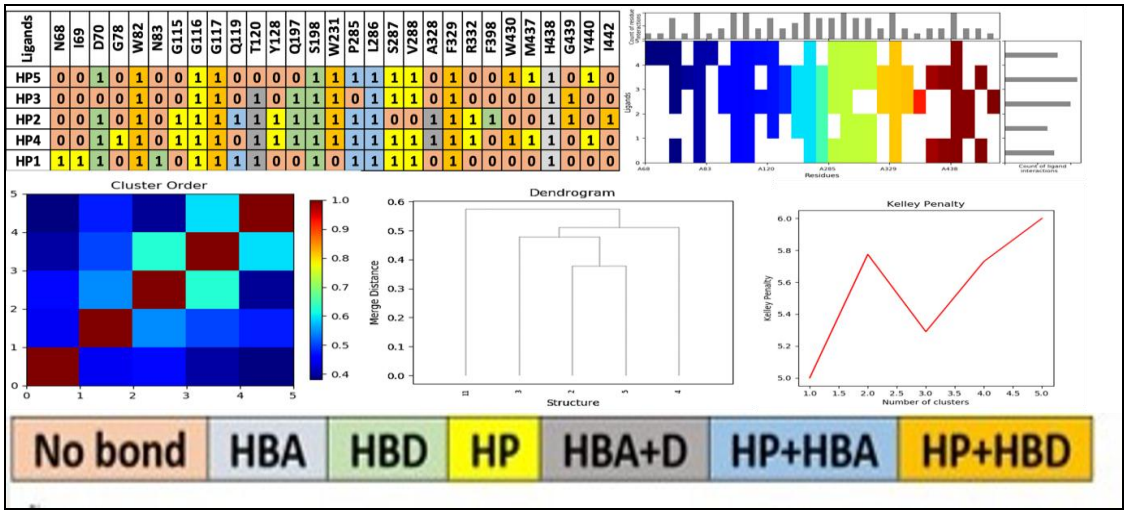

Fig. 5: Structural interaction fingerprinting (Sift) of the selected phytochemicals of *Hypericum perforatum* with BChE enzyme.

SWISS ADME and pkCSM Pharmacokinetic Parameters

Pharmacokinetic properties of the selected phytochemicals from *H. perforatum* were predicted using the pkCSM pharmacokinetics predictive modeling. **Table 2** lists the properties related to absorption, distribution, metabolism, excretion, and toxicity (ADMET) for each phytochemical (HP-1 through HP-5). Likewise, the SwissADME molecular properties of the selected phytochemicals of *H. perforatum* are depicted as heatmap in **Fig. 6**, and the radar plots of the selected phytochemicals of *H. perforatum* obtained from Swiss ADME online tool are shown in **Fig. 7**. The **Table 2** indicates a range of water solubility values, with all compounds showing relatively low solubility (HP-1 and HP-2: -2.892 logS, HP-3: -3.04 logS, HP-4: -3.893 logS, HP-5: -2.925 logS). These solubility values suggest limited bioavailability; however, the Caco-2 permeability data show a range of intestinal absorptivity. HP-4 exhibits the highest Caco-2 permeability (1.055), indicating potential for good intestinal absorption, which is supported by a high predicted human intestinal absorption rate of 98.386%. Conversely, HP-5 shows the lowest intestinal absorption (47.999%) which could limit its oral bioavailability. The skin permeability values are relatively consistent among the compounds, suggesting similar potential for transdermal delivery. P-glycoprotein substrate and inhibition profiles vary, with HP-1, HP-2, and HP-5 identified as substrates and HP-1 also acting as an inhibitor. This could have implications for drug-drug interactions and absorption profiles. Distribution properties, such as the volume of distribution (VDss) and blood-brain barrier (BBB) permeability, reveal the likelihood of each compound to distribute into the human body and cross into the central nervous system (CNS). HP-3 and HP-5 show higher VDss values (1.274 and 1.846, respectively), suggesting a broader distribution. However, BBB permeability is highest for HP-4 (-0.237), indicating a greater propensity for CNS access, which correlates with its higher CNS permeability score (-1.304). Metabolism data suggest none of the compounds are substrates for CYP2D6, which is beneficial for avoiding one common pathway that could lead to drug-drug interactions. HP-3 is the only compound predicted to inhibit CYP1A2, which may necessitate further investigation to assess the clinical significance of this interaction. The excretion parameter, total clearance, provides insight into the rate at which these compounds are removed from the body, with HP-4 showing the highest clearance (0.664 mL/min/kg) and HP-1 the lowest (0.004 mL/min/kg). Toxicity predictions are critical for early safety assessments. All compounds were predicted to be non-toxic in the AMES test and showed no hepatotoxicity or skin sensitization. The hERG II inhibition by HP-1, HP-2, and HP-5 is a concern as it may indicate potential for cardiac toxicity, and these compounds would require careful consideration and further validation in drug development. Maximal tolerated dose (MTD) predictions and acute and chronic oral toxicity data suggest a range of tolerable dosages in humans and rats, with HP-4 showing the highest MTD in humans (0.801 mg/kg) and HP-5 the highest LOAEL in rats (4.417 mg/kg). The minnow toxicity data, especially the high value for HP-5 (8.061), raise questions about environmental impact and necessitate further ecotoxicological evaluation.

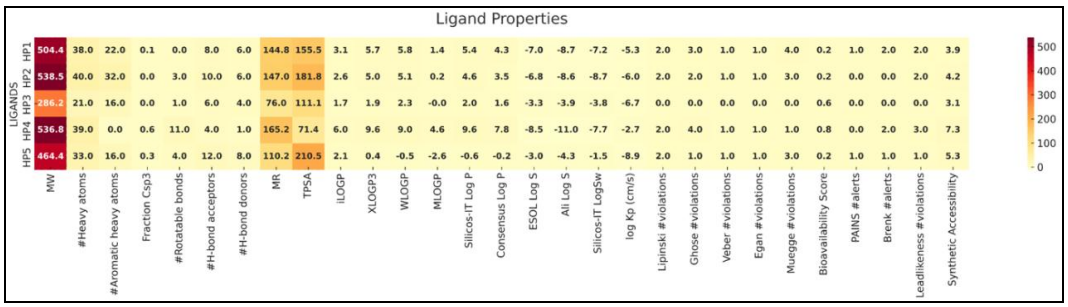

Fig. 6: SwissADME molecular properties of the selected phytochemicals of *Hypericum perforatum.*

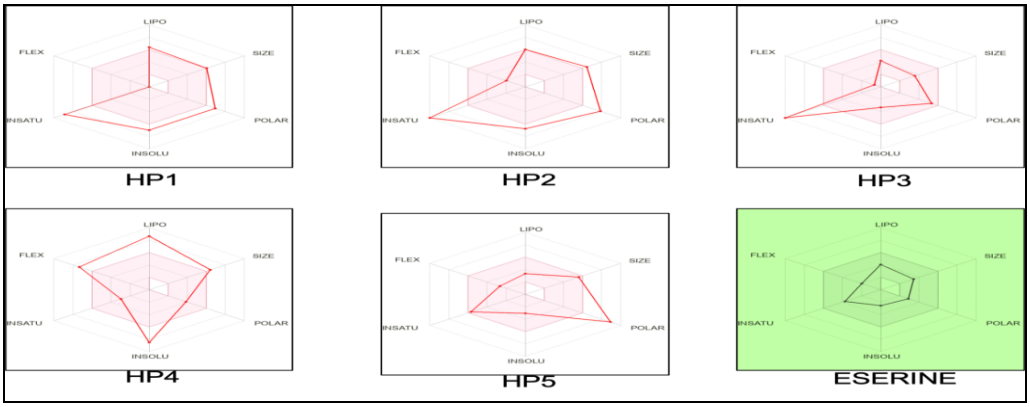

Fig. 7: Radar plots of the selected phytochemicals of *Hypericum perforatum* obtained form Swiss ADME online tool.

Table 2: pkCSM pharmacokinetic parameters of the selected phytochemicals of *Hypericum perforatum.*

Pharmacokinetic Properties		**Selected Phytochemicals**				
Properties	**Model Name**	**HP-1**	**HP-2**	**HP-3**	**HP-4**	**HP-5**
Absorption	**Water solubility**	-2.892	-2.892	-3.04	-3.893	-2.925
	Caco2 permeability	-0.594	-0.111	0.032	1.055	0.242
	Intestinal absorption (human)	100	90.723	74.29	98.386	47.999
	Skin Permeability	-2.735	-2.735	-2.735	-2.715	-2.735
	P-glycoprotein substrate	Yes	Yes	Yes	No	Yes
	P-glycoprotein I inhibitor	Yes	No	No	Yes	No
	P-glycoprotein II inhibitor	Yes	Yes	No	Yes	No
Distribution	**VDss (human)**	-0.734	-1.132	1.274	-0.64	1.846
	Fraction unbound (human)	0.375	0.26	0.178	0	0.228
	BBB permeability	-1.561	-1.659	-0.939	-0.237	-1.688
	CNS permeability	-3.443	-3.283	-2.228	-1.304	-4.093
Metabolism	**CYP2D6 substrate**	No	No	No	No	No
	CYP3A4 substrate	Yes	Yes	No	Yes	No
	CYP1A2 inhibitor	No	No	Yes	No	No
	CYP2C19 inhibitor	No	No	No	No	No
	CYP2C9 inhibitor	No	No	No	No	No
	CYP2D6 inhibitor	No	No	No	No	No
	CYP3A4 inhibitor	No	No	No	No	No
Excretion	**Total Clearance**	0.004	0.421	0.477	0.664	0.394
	Renal OCT2 substrate	No	No	No	No	No
Toxicity	**AMES toxicity**	No	No	No	No	No
	Max. tolerated dose (human)	0.438	0.438	0.531	0.801	0.569
	hERG I inhibitor	No	No	No	No	No
	hERG II inhibitor	Yes	Yes	No	No	Yes
	Oral Rat Acute Toxicity (LD50)	2.482	2.5	2.449	2.043	2.541
	Oral Rat Chronic Toxicity (LOAEL)	2.421	2.918	2.505	2.299	4.417
	Hepatotoxicity	No	No	No	No	No
	Skin Sensitization	No	No	No	No	No
	***T.Pyriformis* toxicity**	0.285	0.285	0.312	0.286	0.285
	Minnow toxicity	2.015	3.538	2.885	-1.887	8.061

StopTox Toxicity Assessment

The toxicity profiles of the selected *H. perforatum* phytochemicals were assessed using the StopTox toxicity prediction tool, with results summarized in **Table 3**. This assessment covers a range of toxicity endpoints, including acute inhalation, oral, dermal, eye irritation and corrosion, skin sensitization, and skin irritation and corrosion. The StopTox toxicity parameters (**Table 3**) indicate a favorable safety profile for HP1, with no toxicity observed across most endpoints except for eye irritation and corrosion. However, HP2 and HP3 exhibit acute dermal toxicity, with HP2 also being a skin sensitizer, which raises concerns regarding their safety in topical applications. HP4 stands out as a skin sensitizer with a positive indication of skin irritation and corrosion, suggesting a potential for adverse dermal reactions. HP5, like HP1, appears to be largely non-toxic except for acute dermal toxicity. These findings highlight the necessity for cautious formulation development, especially for topical applications, and underscore the importance of conducting in-depth in vivo toxicity studies to confirm these predictions and evaluate the risk of adverse effects in humans.

Bioactivity Score Evaluation and drug target prediction

The bioactivity scores of the phytochemicals were evaluated using the online tool Molinspiration, as shown in **Table 4**. These scores predict the potential of the compounds to act as bioactive ligands for various drug targets, including G protein-coupled receptors (GPCRs), ion channels, kinases, nuclear receptors, proteases, and enzymes. As per the bioactivity scores (**Table 4**), HP1 shows promise as a nuclear receptor ligand (score: 0.31) and enzyme inhibitor (score: 0.30), suggesting potential utility in modulating gene expression and enzyme activity. HP2, while demonstrating modest scores, may still possess some activity as a kinase inhibitor (score: 0.12) and GPCR ligand (score: 0.01). HP3 presents as a kinase inhibitor (score: 0.21) and nuclear receptor ligand (score: 0.32), indicating a capacity for signaling modulation and regulation of transcriptional activities. HP4 has a notable score as a nuclear receptor ligand (score: 0.57), which could be significant for therapeutic applications involving hormone receptors. Finally, HP5 exhibits a strong score as an enzyme inhibitor (score: 0.42), suggesting it might be an effective modulator of enzymatic pathways. The varying bioactivity scores of these phytochemicals underscore the chemical diversity within *H. perforatum* and their potential as lead compounds for drug discovery. These preliminary in silico assessments can guide the prioritization of compounds for further experimental validation, thereby streamlining the drug development process. Similarly, the prediction of drug target classes of the selected phytochemicals of *H. perforatum* is presented in **Fig. 8**.

Table 3: StopTox toxicity parameters of the selected phytochemicals of *Hypericum perforatum*

Ligands	Acute Inhalation Toxicity	Acute Oral Toxicity	Acute Dermal Toxicity	Eye Irritation and Corrosion	Skin Sensitization	Skin Irritation and Corrosion
HP1	No	No	No	Toxic	Non sensitizer	Negative
HP2	No	No	Toxic	Toxic	Sensitizer	Negative
HP3	No	No	Toxic	No	Sensitizer	Negative
HP4	No	No	No	No	Sensitizer	Positive
HP5	No	No	Toxic	No	Non sensitizer	Negative

Table 4: Bioactivity score values of the selected phytochemicals of *Hypericum perforatum* assessed by online tool Molinspiration.

Phytocompounds	Parameters of Bioactivity Score					
	GPCR ligand	Ion channel Modulator	Kinase Inhibitor	Nuclear Receptor ligand	Protease Inhibitor	Enzyme Inhibitor
HP-1	0.16	-0.04	-0.02	0.31	0.03	0.30
HP-2	0.01	-0.29	0.12	0.14	-0.02	0.14
HP-3	-0.10	-0.21	0.21	0.32	-0.27	0.26
HP-4	-0.10	-0.20	-0.44	0.57	-0.01	0.25
HP-5	0.06	-0.04	0.13	0.20	-0.06	0.42

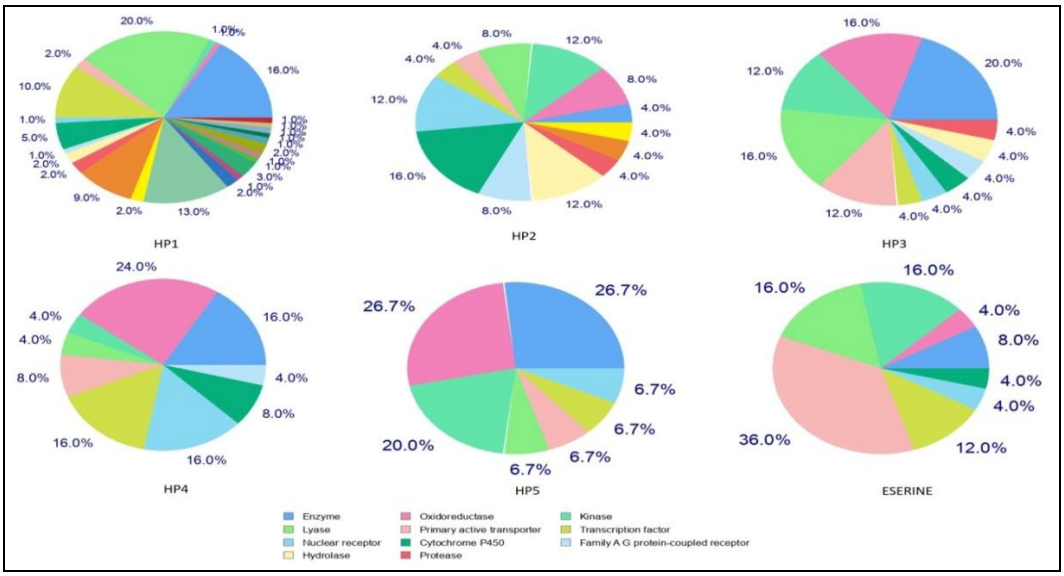

Fig. 8: Prediction of drug target classes of the selected phytochemicals of *Hypericum perforatum.*

DFT Analysis

Table 5 presents the Density Functional Theory (DFT) computational analysis for a series of phytochemicals isolated from *H. perforatum*. It lists numerical values for several electronic parameters, which are pivotal for understanding the reactivity and interaction potential of these compounds with biological targets. The optimized structures of the selected phytochemicals of *H. perforatum* are shown in **Fig. 9**. Similarly, the MESP (ESP and HOMO–LUMO structures with energy gaps) and Molecular Orbital Energies analysis of the selected phytochemicals of *H. perforatum* in aqueous and gas phase is depicted in the **Fig. 10**. The DFT parameters include dipole moment, frontier molecular orbital energies (HOMO and LUMO), energy gap, ionization potential, electron affinity, electronegativity, electrochemical potential, hardness, softness, and electrophilicity index are listed in **Table 5**. The results delineate a wide range of electronic characteristics. HP1 displays a notably high dipole moment (13.875 Debye), suggesting substantial polarity which may affect interactions with polar environments. The HOMO energy level of HP1 is -0.1885 a.u., and the LUMO is -0.102 a.u., resulting in an energy gap (ΔE_Gap) of 2.3516 eV. This compound also has a high ionization potential (5.1283 eV) and electron affinity (2.7767 eV), indicating its potential stability and reactivity. The electronegativity (χ) for HP1 is calculated at 3.9525 eV, with a corresponding electrochemical potential (μ) of -3.9525 eV. Its hardness (η) is 2.3516 eV, and

softness (S) is 0.4252 eV^(-1), while the electrophilicity index (ω) stands at 3.3215 eV. HP2, with a lower dipole moment of 12.352 Debye compared to HP1, exhibits a HOMO energy of -0.2094 a.u. and a LUMO energy of -0.072 a.u. It has a wider energy gap of 3.7367 eV, potentially indicating greater stability. The ionization potential for HP2 is slightly lower than that of HP1 at 5.6967 eV, and it has an electron affinity of 1.96 eV. Its electronegativity value is 3.8284 eV, the electrochemical potential is -3.8284 eV, and it is characterized by a hardness of 3.7367 eV, softness of 0.2676 eV^(-1), and an electrophilicity index of 1.9612 eV. HP3 shows a dipole moment of 9.4844 Debye and has HOMO and LUMO values of -0.2058 a.u. and -0.0573 a.u., respectively. It has an energy gap of 4.0412 eV, an ionization potential of 5.6007 eV, and an electron affinity of 1.5595 eV. The electronegativity is 3.5801 eV, electrochemical potential is -3.5801 eV, hardness is 4.0412 eV, softness is 0.2475 eV^(-1), and electrophilicity index is 1.5858 eV. The compound HP4, with a dipole moment of 7.3363 Debye, HOMO at -0.2218 a.u., and LUMO at -0.0527 a.u., shows an energy gap of 4.6004 eV. This suggests a potentially lower reactivity profile, supported by an ionization potential of 6.0355 eV, electron affinity of 1.4351 eV, electronegativity of 3.7353 eV, electrochemical potential of -3.7353 eV, hardness of 4.6004 eV, softness of 0.2174 eV^(-1), and an electrophilicity index of 1.5165 eV. Lastly, HP5 has a dipole moment of 10.526 Debye with HOMO and LUMO levels at -0.2093 a.u. and -0.0596 a.u., respectively, and an energy gap of 4.0735 eV. Its ionization potential is 5.6959 eV, electron affinity is 1.6223 eV, electronegativity is 3.6591 eV, electrochemical potential is -3.6591 eV, hardness is 4.0735 eV, softness is 0.2455 eV^(-1), and it has an electrophilicity index of 1.

Table 5: DFT and Quantum chemical parameters of the selected phytochemicals of *Hypericum perforatum*.

Ligands	Parameters for DFT analysis										
	Dipole moment (Debye)	HOMO (a.u.)	LUMO (a.u.)	Energy Gap (ΔE_{Gap})	Ionization Potential (eV)	Electron affinity (eV)	Electronegativity χ (eV)	Electrochemical potential μ (eV)	Hardness η (eV)	Softness S (eV)	Electrophilicity ω (eV)
Solvent phase (Aqueous)											
HP1	13.875	-0.1885	-0.102	2.3516	5.1283	2.7767	3.9525	-3.9525	2.3516	0.4252	3.3215
HP2	12.352	-0.2094	-0.072	3.7367	5.6967	1.96	3.8284	-3.8284	3.7367	0.2676	1.9612
HP3	9.4844	-0.2058	-0.0573	4.0412	5.6007	1.5595	3.5801	-3.5801	4.0412	0.2475	1.5858
HP4	7.3363	-0.2218	-0.0527	4.6004	6.0355	1.4351	3.7353	-3.7353	4.6004	0.2174	1.5165
HP5	10.526	-0.2093	-0.0596	4.0735	5.6959	1.6223	3.6591	-3.6591	4.0735	0.2455	1.6434
Gas phase											
HP1	8.827	0.186	-0.0951	-7.6515	-5.0613	2.59025	-1.2355	1.23553	-7.6515	-0.1306	-0.0997
HP2	8.8362	-0.1970	-0.0698	3.46074	5.36091	1.90017	3.63054	-3.6305	3.46074	0.28895	1.90433
HP3	6.9736	-0.1997	-0.0501	4.07055	5.43438	1.36383	3.39911	-3.3991	4.07055	0.24566	1.41921
HP4	5.218	-0.2127	-0.0434	4.60716	5.78840	1.18124	3.48482	-3.4848	4.60716	0.21705	1.31795
HP5	7.798	-0.1967	-0.0463	4.09177	5.35384	1.26206	3.30795	-3.3079	4.09177	0.24439	1.33714

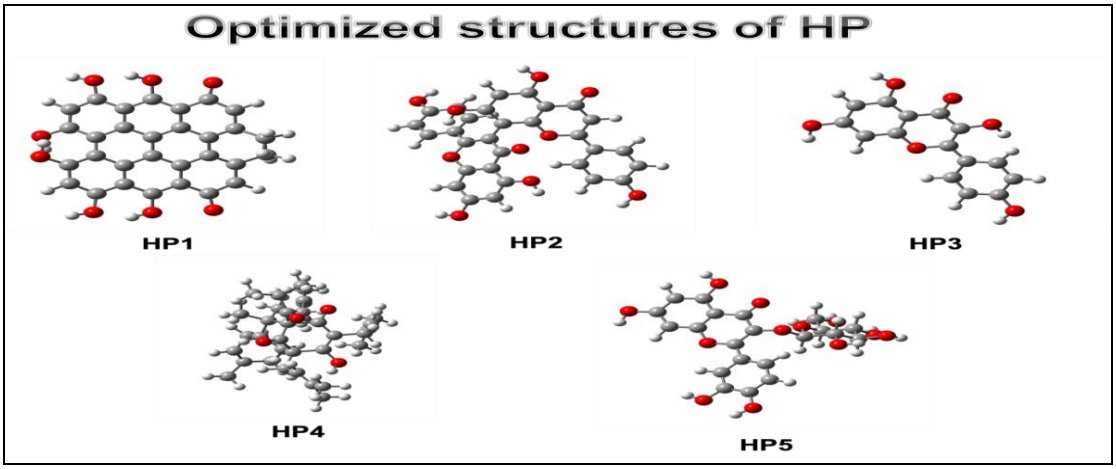

Fig. 9: Optimized structures of the selected phytochemicals of *Hypericum perforatum.*

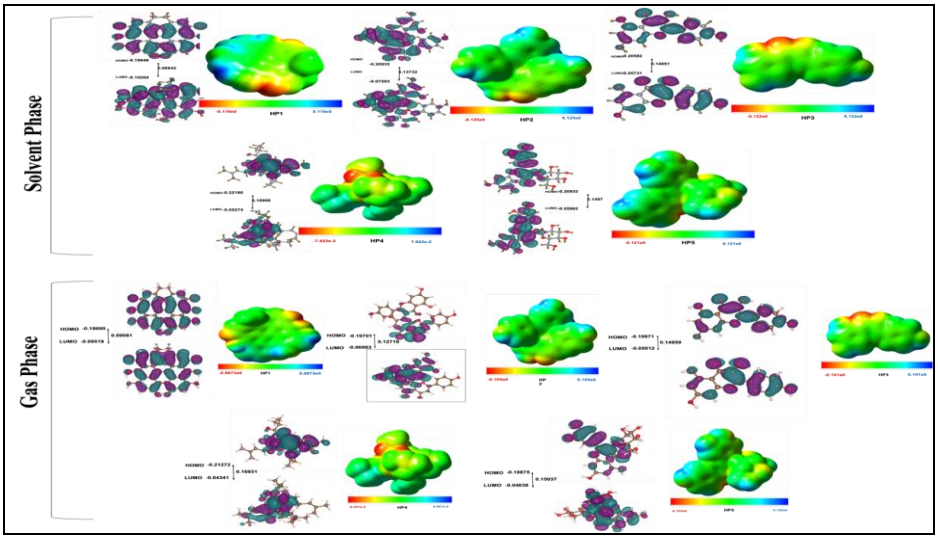

Fig. 10: MESP (ESP and HOMO–LUMO structures with energy gaps) and Molecular Orbital Energies analysis of the selected phytochemicals of *Hypericum perforatum* in aqueous and gas phase.

MD simulation result analysis

HP-2 and HP-5 were selected as the primary targets for AChE and BChE, respectively, based on their exceptional docking scores and subsequent participation in a molecular dynamics simulation study. Molecular dynamics (MD) simulations were conducted in order to assess the stability of the protein-ligand complex. The study assessed the alterations in protein structure induced by ligands. The stability and mobility of the docked complexes were evaluated by molecular dynamics (MD) simulations conducted on the iMod server. The study examined the sluggish behavior of the docked complexes and demonstrated their significant conformational changes using NMA[27]. The B-factor, sometimes referred to as main-chain deformability, quantifies the capacity of molecules to undergo twisting at individual residues (**Fig. 11** and **12** depict the B-factor graph). The B-factor graphs present a comparison between the NMA and PDB domains of the complexes. The covariance matrices of the 3S7S–C1 complex demonstrate the correlation among the residues within the complex. In the matrix, the white hue signifies motion that is not associated, whereas the red color indicates a strong correlation between residues. Furthermore, the hue blue demonstrates anticorrelations. The system's complexity increases as correlation increases. The elastic maps of the docked proteins depict the interatomic interactions, with the deeper gray areas indicating regions of higher stiffness (**Fig. 11** and **Fig. 12 (E, F)**). These Figures represents critical outputs from molecular dynamics simulations that analyze the structural dynamics of the AChE-HP-2 and BChE-HP-5 complexes. The deformability graph (A) indicates which parts of the protein may experience structural changes upon ligand binding, reflecting regions of potential flexibility or structural constraint. The B-factor plot (B) parallels experimental temperature factors, providing insights into regions of the molecule that are more dynamically active in the simulation. Variance (C) quantifies the extent of fluctuation in the atomic positions, suggesting how binding affects the structural integrity of the complex. Eigenvalues (D) are a statistical measure of the movement's magnitude within the protein-ligand complex, with lower values indicating larger, more significant motions that could be critical for the function or inhibition of AChE by the ligand. The elastic network model (E) visualizes the inter-residue connections, which are crucial for maintaining the protein's 3D structure upon ligand interaction, while the covariance matrix (F) provides a deeper understanding of the correlated motions between different parts of the complex, important for understanding allosteric effects or conformational changes upon ligand binding. These results collectively offer a comprehensive view of the dynamic behavior of the complex and are essential for elucidating the molecular basis of the inhibitor's action.

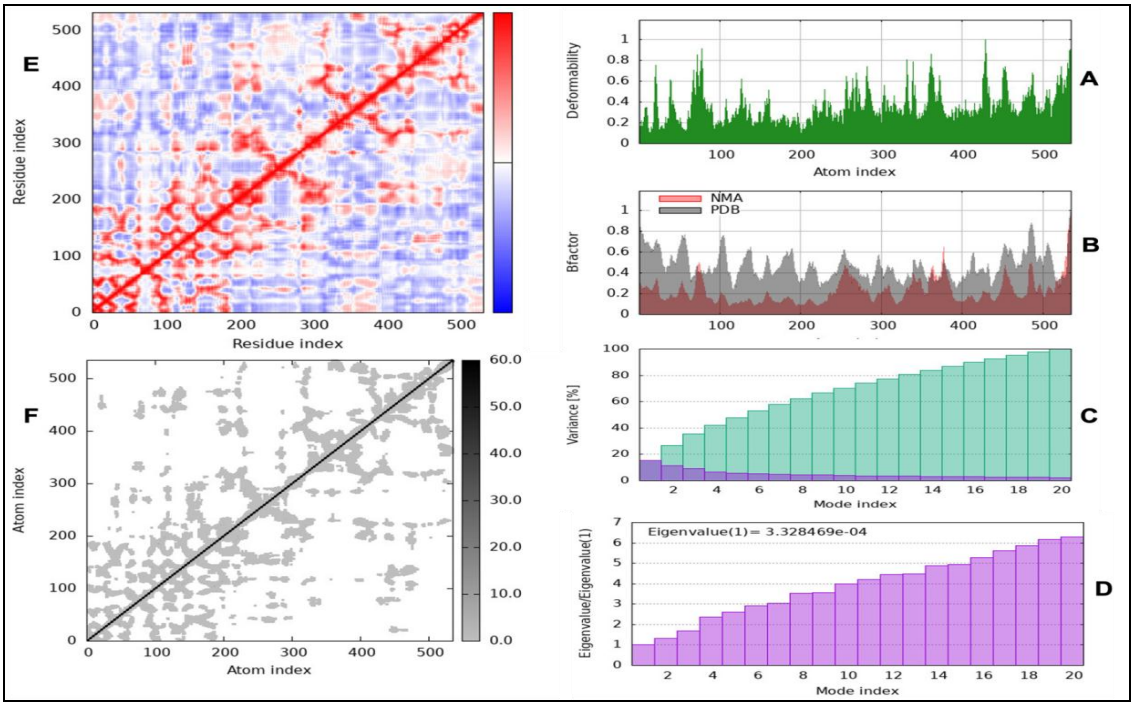

Fig. 11: Outputs of MD simulations through iMODS for AChE-HP2 complex: (A) deformability; (B) B-factor plot; (C) variance plot; (D) eigenvalue; (E) elastic network model; (F) covariance.

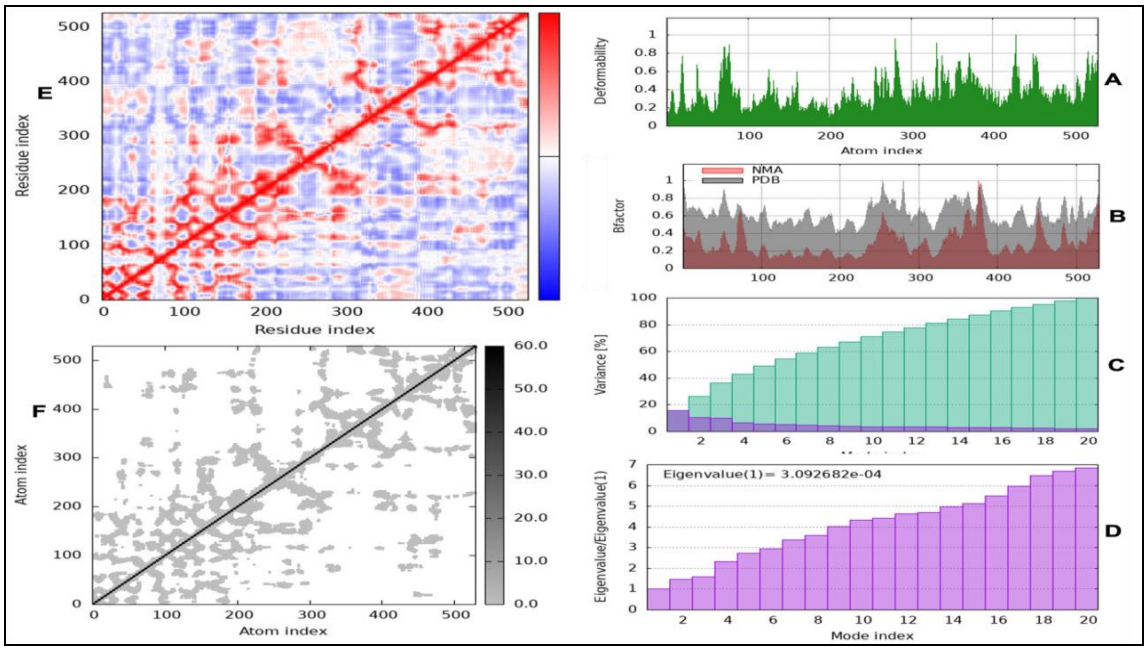

Fig. 12: Outputs of MD simulations through iMODS for BChE-HP5 complex: (A) deformability; (B) B-factor plot; (C) variance plot; (D) eigenvalue; (E) elastic network model; (F) covariance.

Conclusion

The current extensive study concludes four phytochemicals, namely, hypericin (HP-1), biapigenin (HP-2), kaempferol (HP-3), hyperforin (HP-4), hyperocide (HP-5) as potential inhibitors against the AChE and BChE enzymes. The findings of the combined molecular docking and molecular dynamics (MD) simulation investigation indicate that the bioactive compounds exhibit a very stable complex with the targeted proteins, demonstrating superior binding affinities compared to other chemicals obtained from sesame. Furthermore, the possible inhibitors that have been suggested also satisfy the requirements of drug similarity as determined

by Lipinski's rule of five and ADME characteristics. Overall, this comprehensive analysis elucidates the complex phytochemical landscape of *H. perforatum*, highlighting its potential neuro-pharmacological benefits. The favorable pharmacokinetics and safety profiles, coupled with promising interaction dynamics with key enzymes, underscore the therapeutic potential of *H. perforatum's* constituents. Our study paves the way for further research and development of phytochemical-based therapeutics, contributing to the expanding arsenal of natural compounds in modern medicine.

REFERENCES

1. Zhang, H. and Z. Ma, "Phytochemical and pharmacological properties of Capparis spinosa as a medicinal plant", ***Nutrients***, 10(2), 116 (2018).
2. M. Locatelli, G. Zengin, A. Uysal, *et al.,* "Multicomponent pattern and biological activities of seven Asphodeline taxa: potential sources of natural-functional ingredients for bioactive formulations", ***J Enzyme Inhib Med Chem***, 32(1), 60-67 (2017).
3. M. Gunjan, T. Naing, *et al.,* "Marketing trends & future prospects of herbal medicine in the treatment of various disease", ***World J Pharm Res***, 4(9), 132-155 (2015).
4. C. Ballard, S. Gauthier, A. Corbett, *et al.,* "Alzheimer's disease", ***Lancet***, 377(9770), 1019-1031 (2011).
5. D. Ferreira, L. Perestelo-Pérez, E. Westman, *et al.,* "Meta-review of CSF core biomarkers in Alzheimer's disease: the state-of-the-art after the new revised diagnostic criteria", ***Front Aging Neurosci***, 6, 47 (2014).
6. S.K. Yusufzai, M. S. Khan , O. Sulaiman , *et al.,* "Molecular docking studies of coumarin hybrids as potential acetylcholinesterase, butyrylcholinesterase, monoamine oxidase A/B and β-amyloid inhibitors for Alzheimer's disease", ***Chem Cent J***, 12(1), 1-57 (2018).
7. J.T. Abraham, , H.N.S. Maharifa, and S. Hemalatha, "In silico molecular docking approach against enzymes causing Alzheimer's disease using Borassus flabellifer Linn.", ***Appl Biochem Biotechnol***, 1-10 (2022).
8. J.Hardy, "A hundred years of Alzheimer's disease research", ***Neuron***, 52(1), 3-13 (2006).
9. M.V. Suryawanshi, P. P. Gujarathi, T. Mulla, *et al.,* "Hypericum perforatum: a comprehensive review on pharmacognosy, preclinical studies, putative molecular mechanism, and clinical studies in neurodegenerative diseases", ***N-S ARCH PHARMACOL,*** 1-16 (2024).
10. K. Hosni, K. Msaâda, M. B. Taârit, *et al.,* "Essential oil composition of Hypericum perfoliatum L. and Hypericum tomentosum L. growing wild in Tunisia", ***Ind Crops Prod***, 27(3), 308-314 (2008).
11. S.J.Y.Macalino, V. Gosu, S. Hong , *et al.,* "Role of computer-aided drug design in modern drug discovery", ***Arch Pharm Res***, 38(9), 1686-1701 (2015).
12. M.M.Alom, R. Parvin Bonna, A. Islam , *et al.,* "Unveiling neuroprotective potential of spice plant-derived compounds against alzheimer's disease: insights from computational studies", ***Int J Alzheimers Dis***, 2023, 8877757 (2023).
13. F.Stanzione, I. Giangreco, and J.C. Cole, "Use of molecular docking computational tools in drug discovery", ***Prog Med Chem***, 60, 273-343 (2021).
14. R.A. Friesner, J. L. Banks, R. B. Murphy, *et al.,*"Glide: a new approach for rapid, accurate docking and scoring. 1. Method and assessment of docking accuracy", ***J Med Chem***, 47(7), 1739-1749 (2004).
15. Y. Pan, Y. Wang, and S.H. Bryant, "Pharmacophore and 3D-QSAR characterization of 6-arylquinazolin-4-amines as Cdc2-like kinase 4 (Clk4) and dual specificity tyrosine-phosphorylation-regulated kinase 1A (Dyrk1A) inhibitors", ***J Chem Inf Model***, 53(4), 938-947 (2013).
16. S.K. Tripathi, S. K. Singh, P. Singh, *et al.,* "Exploring the selectivity of a ligand complex with CDK2/CDK1: a

molecular dynamics simulation approach", ***J Mol Recognit***, 25(10), 504-512 (2012).
17. A.J. Owoloye, F. C. Ligali,O. A. Enejoh, *et al.,* "Molecular docking, simulation and binding free energy analysis of small molecules as Pf HT1 inhibitors", ***PLoS One***, 17(8), e0268269 (2022).
18. S. Hamza, A. Abid, A. Khanum *et al.*, "3D-QSAR, docking and molecular dynamics simulations of novel Pyrazolo-pyridazinone derivatives as covalent inhibitors of FGFR1: a scientific approach for possible anticancer agents", ***J Biomol Struct Dyn***,1-15 (2023).
19. K.K. Kakarala, K.J.J.o.R. Jamil, and S. Transduction, "Screening of phytochemicals against protease activated receptor 1 (PAR1), a promising target for cancer", ***J Recept Signal Transduct*** 35(1) 26-45 (2015).
20. L.Mittal, A. Kumari, M. Srivastava, *et al.,* "Identification of potential molecules against COVID-19 main protease through structure-guided virtual screening approach", ***J Biomol Struct Dyn***, 39(10), 3662-3680 (2021).
21. I. Habib, T. A. Chohan, T. A. Chohan, *et al.,* "Integrated Computational Approaches for Designing Potent Pyrimidine-Based CDK9 Inhibitors: 3D-QSAR, Docking, and Molecular Dynamics Simulations", ***Comput Biol Chem***, 108, 108003 (2023).
22. A. Daina, O. Michielin, and V. Zoete, ***Sci Rep***, 7, 42717 (2017).
23. D.E.Pires, T.L. Blundell, and D.B. Ascher, "pkCSM: predicting small-molecule pharmacokinetic and toxicity properties using graph-based signatures", ***J Med Chem***, 58(9), 4066-4072 (2015).
24. J.V. Borba, V. M. Alves, R. C. Braga, *et al.,* "STopTox: An in silico alternative to animal testing for acute systemic and topical toxicity", ***Environ Health Perspect***, 130(2), 027012 (2022).
25. A. Daina, O. Michielin, and V. Zoete, "SwissTargetPrediction: updated data and new features for efficient prediction of protein targets of small molecules", ***Nucleic Acids Res***, 47(W1), W357-W364 (2019).
26. S.A. Ejaz, A. Saeed, P. R. Birmani, *et al.,* "In-silico Investigations of quinine and quinidine as potential Inhibitors of AKR1B1 and AKR1B10: Functional and structural characterization", ***PLoS One***, 17(10), e0271602 (2022).
27. N. Shafiq, B. Shakoor, N. Yaqoob, *et al.,* "A virtual insight into mushroom secondary metabolites: 3D-QSAR, docking, pharmacophore-based analysis and molecular modeling to analyze their anti-breast cancer potential", ***J Biomol Struct Dyn***, 1-22 (2024).
28. Singh, S. and S. Gaur, "Virtually selected phytochemicals from edible seeds as possible potential medicaments for hypercholesterolemia: an in silico approach", ***J Biomol Struct Dyn***, 41(18) 8690-8700 (2023).
29. G.Schneider, W. Neidhart, T. Giller, *et al.,* "Scaffold-hopping by topological pharmacophore search: a contribution to virtual screening", ***Angew Chem Int Ed***, 38(19), 2894-2896 (1999).
30. J.Venhorst, S. Núñez, J. Willem, *et al.*, "Assessment of scaffold hopping efficiency by use of molecular interaction fingerprints", ***J Med Chem***, 51(11), 3222-3229 (2008).
31. J.B. Jasper, L. Humbeck, T. Brinkjost *et al.,* "A novel interaction fingerprint derived from per atom score contributions: exhaustive evaluation of interaction fingerprint performance in docking based virtual screening", ***J Cheminform***, 10(1), 1-13 (2018).
32. Z. Deng, C. Chuaqui, and J. Singh, "Structural interaction fingerprint (SIFt): a novel method for analyzing three-dimensional protein− ligand binding interactions", ***J Med Chem***, 47(2), 337-344 (2004).

Bull. Pharm. Sci., Assiut University, Vol. 48, Issue 1, 2025, pp. 277-294.

نشرة العلوم الصيدليـــة
جامعة أسيوط

BULL. PHARM. SCI. Assiut Univ.

الكشف عن الفارماكولوجية المحتملة للمركبات المشتقة من عشبة القديس يوحنا ضد مرض الزهايمر: رؤى من الدراسات الحاسوبية والديناميكية Hypericum perforatum

عادل الغامدي*

قسم الكيمياء الصيدلانية ، كلية الصيدلة ، جامعة الباحة ، ص. ب ١٩٨٨ الباحة ، المملكة العربية السعودية

مرض الزهايمر يهدد بشكل كبير نظام الرعاية الصحية في جميع أنحاء العالم ، والذي ينشأ من مجموعة من الحالات التي تؤدي إلى خلل في الخلايا العصبية ، وضعف الذاكرة ، والتدهور المعرفي .

حظيت نبتة القديس يوحنا Hypericum perforatum باهتمام كبير نظرا لمزاياها العلاجية المحتملة في علاج الأمراض التنكسية العصبية. أصبح الافتقار إلى علاجات فعالة لأمراض مثل مرض الزهايمر ومرض الشلل الرعاشي مشكلة صحية عالمية.

بحثت هذه الدراسة في الإمكانات العلاجية لخمس مواد كيميائية نباتية hypericin (HP-1), biapigenin (HP-2), kaempferol (HP-3), hyperforin (HP-4), hyperocide (HP-5)

وقد تم قياس مدي قوة الارتباط مع انزيم أستيل كولينستراز acetylcholinesterase (AChE) وانزيم بوتيريل كولينستراز butyrylcholinesterase (BChE) عن طريق دراسة الإرساء الجزئي باستخدام برنامج The Glide-XP module from Schrödinger لتحديد الطاقات الملزمة لتفاعلاتها مع البروتينات المستهدفة ثم يلي بعد ذلك دراسة المحاكاة الديناميكية الجزيئية باستخدام برنامج IMods. لتأكيد مدي استقرار الارتباط مع البروتينات المستهدفة.

قد اثبتت الدراسات ان اعلي نسبة نجاح وأكبر درجات الالتحام لإنزيم AChE بين المركبات الكيميائية النباتية الخمسة المختارة ، هي مركب HP-1 (-7.304 kcal/mol) and HP-2 (-7.461 kcal/mol) وبالمثل، في حالة إنزيم BChE فإن درجات الالتحام للإنزيم تعد كبيرة للمواد الكيميائية النباتية HP-3 (-7.849 kcal/mol) and HP-5 (-7.991 kcal/mol)

وقد تم ايضا دراسة و فحص خصائص المركبات المختارة من خلال الأدوات المختلفة عبر الإنترنت بما في ذلك swissADME و pkSCM و stoptox و molinspiration.